Electron correlation effects in Auger cascades following $2p^{-1}4s$ excitations in argon

S.-M. Huttula,[1] S. Heinäsmäki,[1] H. Aksela,[1] J. Tulkki,[2] A. Kivimäki,[1] M. Jurvansuu,[1] and S. Aksela[1]
[1]*Department of Physical Sciences, P.O. Box 3000, FIN-90014 University of Oulu, Finland*
[2]*Laboratory of Computational Engineering, Helsinki University of Technology, P.O. Box 9400, FIN-02015 HUT, Finland*
(Received 3 August 2000; published 6 February 2001)

Effects of intermediate coupling and configuration interaction on the partial transition rates, total decay widths, and angular distribution parameters of the Ar resonant Auger transitions $2p^5 4s \rightarrow 3s^1 3p^5 4s$ and of the second-step Auger transitions $3s^1 3p^5 4s(^2P_{1/2,3/2}) \rightarrow 3p^4$ have been studied both theoretically and experimentally. Transition rates and angular anisotropies have been calculated for the first- and second-step transitions using the multiconfiguration Dirac-Fock method. High-resolution spectra of both steps have been measured and used to test different schemes for the description of the many-particle states and the existence of possible coherence effects in the second-step spectra.

DOI: 10.1103/PhysRevA.63.032703 PACS number(s): 32.80.Hd, 32.80.Fb

I. INTRODUCTION

The $2p^{-1}4s \rightarrow 3p^4 4s$ resonant Auger spectra of Ar have been widely studied in the past [1–6]. Much less attention has been paid to the intensity and angular distributions of the resonant Auger transitions

$$2p^6 3s^2 3p^6(^1S_0) + h\nu \rightarrow 2p^5 3s^2 3p^6(^2P_{1/2,3/2})4s, J_0 = 1, \quad (1)$$

$$\rightarrow 2p^6 3s^1 3p^5 4s + e^-. \quad (2)$$

In the Ar $L_{2,3}M_1M_{2,3}$ normal Auger spectrum the single configuration $3s^1 3p^5$ does not represent the final state correctly; it is necessary to include configuration interaction (CI) [7–11]. The mixing between the final state configurations $3s^1 3p^5$, $3s^2 3p^3 3d^1$, $3s^2 3p^3 4s^1$, and $3s^2 3p^3 4d^1$ is strong and changes the structure of the normal Auger spectrum considerably as compared to the single configuration prediction. The same effect has been observed in the Ar $3s$ photoelectron spectrum, in which the mixing of the $3s^{-1}$ and $3p^4 nl$ states produces a rich correlation satellite structure [12,13].

In the first part of this work, we measured the resonant Auger spectra $2p^{-1}4s \rightarrow 3s^1 3p^5 4s$ with very high photon and electron energy resolutions. The energies and angular and intensity distributions of the first-step (resonant) Auger transitions were determined. The effects of electron correlation were studied by using three different calculation methods and by comparing the theoretical and experimental results.

A careful study of electron correlation that affects the population of the states in Eq. (2) is of great interest since these states decay further via second-step Auger transitions

$$2p^6 3s^1 3p^5(^1P_1)4s(^2P_{1/2,3/2}) \rightarrow 2p^6 3s^2 3p^4 + e^-. \quad (3)$$

The cascade process was investigated by means of an electron-electron coincidence experiment previously by von Raven *et al.* [14] and recently by Ueda *et al.* [15,16]. As pointed out by Ueda *et al.*, the energy separation between the two spin-orbit split states $2p^6 3s^1 3p^5(^1P_1)4s(^2P_{1/2})$ and $(^2P_{3/2})$ is much smaller than the natural widths of these states and thus the states are populated coherently via the first-step Auger decay. Ueda *et al.* showed [15,16] that within the nonrelativistic LSJ approximation the lifetime interference effect has an important role in the angular distribution of second-step Auger decay. They also determined the ratio of the s and d Auger decay amplitudes and their phase difference in the resonant Auger transition $2p_{3/2}^{-1}4s \rightarrow 3s^1 3p^5(^1P)4s(^2P)$ from two experiments: first, from a coincidence measurement of the angular correlation between the resonant Auger electron and the subsequent second-step Auger electron and, second, from measurements of the angular distributions of the two electrons separately. The ratio of the amplitudes they obtained was $M_d/M_s = 0.52 \pm 0.15$ and the phase difference $\cos\Delta\phi = 0.01 \pm 0.03$.

In the second part of the present work, the second-step Auger spectra were measured. The angular and intensity distributions of these second-step transitions were calculated, and the results are compared with experiments. The effects of the electron correlation in the cascade process are studied, and the limits of the LSJ approximation are discussed.

II. EXPERIMENT

The experiments were performed on the new undulator beamline I411 at the 1.5 GeV MAX-II storage ring at Lund, Sweden. Radiation in the photon energy range from 50 eV to well above 1000 eV is monochromatized by a modified SX-700 plane grating monochromator [17]. The resonant Auger and second-step Auger spectra were measured with photon energies $h\nu = 244.4$ eV and $h\nu = 246.5$ eV, corresponding to the Ar $2p_{3/2} \rightarrow 4s$ and $2p_{1/2} \rightarrow 4s$ resonances, respectively. The ejected electrons were recorded with a rotatable SES-200 hemispherical analyzer [18] at the angles 0 °, 54.7 °, and 90 ° with respect to the polarization direction of the incident radiation. For the resonant Auger measurements, a 20 eV pass energy was used, which corresponds to a kinetic energy resolution of about 30 meV, while the second-step Auger spectra were taken with 10 eV pass energy (kinetic energy resolution ~15 meV). The photon energy resolution was about 35 meV in the resonant Auger spectra and about 100 meV in the second-step Auger spectra. The former is narrower than the lifetime widths of $2p_{3/2} \rightarrow 4s$ and $2p_{1/2} \rightarrow 4s$ resonances (114 meV and 109 meV [19]). Hence line nar-

rowing occurs in the first-step decay spectra due to the Auger resonant Raman effect [20].

For angular distribution measurements, the spectrometer can be rotated in a plane perpendicular to the direction of the photon beam. The asymmetry parameter β can be determined from measurements performed at three angles. The resonant Auger spectra were energy calibrated using the $3s$ photoelectron line, whose binding energy is 29.240 eV [21]. The kinetic energy scale of the second-step spectra was calibrated with the aid of the $3s^1 3p^5(^1P)4s$ peak in the resonant Auger spectrum and the optical energies for the $3p^4$ states [21]. The differences in the transmission of the electron analyzer at the three angles were found to be negligibly small ($\leqslant 5\%$); hence no transmission correction was performed.

III. CALCULATIONS

The energy difference between the resonant states $2p_{3/2}^{-1}4s$ and $2p_{1/2}^{-1}4s$ is much larger than the natural width of these states and thus they can be excited separately. Therefore a two-step model can be used for the resonant Auger decay. The Auger decay rate from an initial state i to a final state f is then given by

$$\frac{dW_{i\to f}(\theta)}{d\omega} = \frac{W_{i\to f}}{4\pi}[1+\beta P_2(\cos\theta)], \tag{4}$$

where θ is the angle between the direction of the polarization vector of the incoming radiation and the direction of Auger electrons and $P_2(\cos\theta)$ is the second-order Legendre polynomial. Reflecting the two-step nature of the decay, the angular distribution parameter β is given as a product of two factors, $\beta = \mathcal{A}_{20}\alpha_2$. In the dipole approximation, the second-rank statistical tensor $\mathcal{A}_{20}$ (the alignment parameter) completely describes the population of magnetic JM sublevels of the core excited state. Using linearly polarized light, photoexcitation from a $J_{gr}=0$ ground state to a $J_0=1$ state results in an energy-independent value of $-\sqrt{2}$ for the alignment. The energies and eigenvectors for the states involved in the cascade process were calculated using the GRASP code [22]. The continuum orbitals were calculated in the jj-averaged field of the core and spectator electrons and they were made orthogonal to the bound orbitals using Lagrangian multipliers. The bound orbitals were optimized for the final state and kept frozen during Auger decay. The energies that were obtained as differences between the separately optimized initial and final state atomic state functions were used in the calculation of the transition amplitudes. For details of our computational approach, see Refs. [23,24].

The angular distribution parameters for the cascade process (1), (2), and (3) were calculated both by using the two-step model and by including the lifetime interference effect in the calculations. When the first-step Auger electron is not detected the angular distribution of the Auger electron emission in the second-step decay can be described, using the general expression [25], as

$$W(\theta) = \frac{C}{4\pi}\sum_{k,J,J'} A_k(J,J',J_f)\rho_{k0}(J,J') \times \frac{\Gamma_{JJ'}}{\omega_{JJ'}^2+\Gamma_{JJ'}^2} P_k(\cos\theta) \tag{5}$$

with $k=0,2,4,\ldots$. Here $\rho_{k0}(J,J')$ are the statistical tensors describing the overlapping states with total angular momenta J and J' immediately after the first decay, J_f is the total angular momentum of the cascade final state, $\omega_{JJ'}=E_J-E_{J'}$ is the energy splitting of these levels, $\Gamma_{JJ'}=\frac{1}{2}(\Gamma_J+\Gamma_{J'})$ with Γ_J being the total width of the level J, $P_k(x)$ is the Legendre polynomial, and C is a constant factor. If the final state fine structure is not resolved by experiment, Eq. (5) should be summed over J_f because the contributions of different final states are incoherent. The coefficients $A_k(J,J',J_f)$ in Eq. (5) read, using the abbreviation $\hat{x} \equiv \sqrt{2x+1}$,

$$A_k(J,J',J_f) = (-1)^{J+J_f-1/2}\sum_{l,l',j,j'} \hat{l}\hat{l}'\hat{j}\hat{j}'\hat{J}\hat{J}'\langle l0l'0|k0\rangle \times \begin{Bmatrix} j & J & J_f \\ J' & j' & k \end{Bmatrix}\begin{Bmatrix} j & l & 1/2 \\ l' & j' & k \end{Bmatrix} \times \langle J_f, lj:J||V||J\rangle\langle J_f, l'j':J'||V||J'\rangle^* \tag{6}$$

and

$$\rho_{k0}(J,J') = \rho(J_0,J_0)\sum_{j_1} \hat{J}_0^2(-1)^{j_1+J_0+J}\begin{Bmatrix} J_0 & J & j_1 \\ J' & J_0 & k \end{Bmatrix} \times \langle J, lj||V||J_0\rangle\langle J', lj||V||J_0\rangle^*, \tag{7}$$

where $\rho_{k0}(J_0,J_0)$ are the statistical tensors of the initial resonant state, and the amplitudes $\langle J,lj||V||J_0\rangle$ describe the first-step Auger decay [15].

The angular distribution parameters and transition rates were calculated for both the first-step and cascade Auger transitions using three different calculation methods for the states involved in the decay process. First, the states were calculated using a single-configuration Dirac-Fock calculation in the ''nonrelativistic'' limit (NRL). Here the value used for the speed of light is increased, which suppresses the small components of the one-particle spinors. Second, the intermediate-coupling (IC) method was used. The effect due to the mixing of the configurations was investigated by using the multiconfiguration (MC) method. A basis set including the $2p^6 3s^1 3p^5 4s^1$, $2p^6 3s^1 3p^5 3d^1$, $2p^6 3s^2 3p^3 4s^1 3d^1$, and $2p^6 3s^2 3p^3 3d^2$ configurations was used for the final states of the first-step decay.

Channel mixing was completely omitted in our calculations. In a previous study [23], channel interaction was found to affect the angular anisotropy of normal Auger transitions significantly, and sometimes even to change the sign.

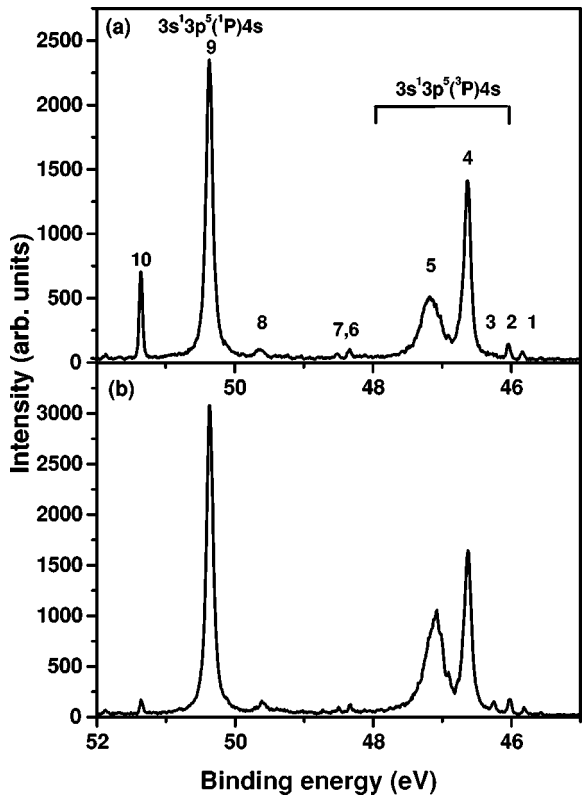

FIG. 1. The $2p^{-1}4s \rightarrow 3s^1 3p^5 4s$ resonant Auger spectra of Ar excited at (a) $h\nu = 246.5$ eV corresponding to the $2p_{1/2}^{-1}4s$ excitation and (b) $h\nu = 244.4$ eV corresponding to the $2p_{3/2}^{-1}4s$ excitation. The spectra were measured at 54.7 ° upward from the electric vector of the incident light. Line numbers refer to Table I.

IV. RESULTS AND DISCUSSION

A. The resonant Auger (first-step) transitions

1. Experimental results

Figure 1 shows the resonant Auger spectra following the Ar $2p_{3/2} \rightarrow 4s$ and $2p_{1/2} \rightarrow 4s$ resonant excitations in the binding energy region 45–52 eV, measured at the angle 54.7 °. This energy region includes the resonant Auger transitions to the $3s^1 3p^5 4s$ states. In a previous study [12] it was suggested that the peaks in the binding energy region 46.5–47.5 eV originate from the transitions to the $3s^1 3p^5 (^3P) 4s$ states and the peak at 50.37 eV binding energy originates from the transitions to the $3s^1 3p^5 (^1P) 4s$ states. In order to determine the relative line intensities at each angle, the spectra were least-squares fitted using Voigt functions. The intensities were normalized by assuming that the β parameters of the $2p^{-1}4s \rightarrow 3p^{-2}4s$ transitions [6] are known. Only the spectra measured at the angles 54.7 ° and 90 ° were used for the determination of β parameters since there was some uncertainty in the normalization of the spectra measured at 0 °. The experimental energies, relative intensities, and angular distribution parameters of the resonant Auger lines are shown in Table I. The intensities in Table I are given relative to the $3s^1 3p^5 (^1P) 4s (^2P_{1/2,3/2})$ line.

2. Results of calculations and comparison with experiment

The excited state includes in the LSJ coupling two terms $2p^5 4s (^1P_1, ^3P_1)$ and in the resonant Auger final state seven terms $3s^1 3p^5 (^3P) 4s (^4P_{5/2,3/2,1/2})$, $3s^1 3p^5 (^3P) 4s (^2P_{3/2,1/2})$, and $3s^1 3p^5 (^1P) 4s (^2P_{1/2,3/2})$. According to the MC calculations, the excited states are intermediate-coupling states, which are linear combinations of the LSJ states as follows: $'|^1P_1\rangle' = 0.8114|^1P_1\rangle + 0.5845|^3P_1\rangle$ and $'|^3P_1\rangle' = 0.8114|^3P_1\rangle - 0.5845|^1P_1\rangle$. The $3s^1 3p^5 4s$ states are quite well described by one LSJ term in a single-configuration picture.

The calculated $2p_{3/2}^{-1}4s \rightarrow 3s^1 3p^5 4s$ resonant Auger spectra are shown together with the experimental spectrum in Fig. 2. The resonant Auger spectrum following the $2p_{3/2} \rightarrow 4s$ excitation obtained from the NRL calculation shows only two peaks [Fig. 2(d)], which correspond to the $3s^1 3p^5 (^1P) 4s$ and $3s^1 3p^5 (^3P) 4s$ peaks in the experimental spectrum. The energy splitting of the peaks is about 8 eV, which is much larger than the experimental splitting. In intermediate coupling [Fig. 2(c)], the $3s^1 3p^5 (^3P) 4s$ peak is divided into two components, which are also resolved in the experimental spectrum. The energy splitting of the $(^1P) 4s$ and $(^3P) 4s$ peaks is smaller and thus closer to the experimental values than in the NRL calculation.

The energy splitting of the $(^3P) 4s$ and $(^1P) 4s$ peaks in the MC calculation [Fig. 2(b)] is much closer to the experi-

TABLE I. Experimental energies, intensities, and β parameters for the $2p^{-1}4s \rightarrow 3s^1 3p^5 4s$ transitions.

			$2p_{1/2}^{-1}4s$			$2p_{3/2}^{-1}4s$		
No.	Energy	Final state	Rel. intensity	β	Ref. [26]	Rel. intensity	β	Ref. [16]
1	45.84		1.3(3)	0.41(7)		1.1(3)	0.47(6)	
2	46.03		3.3(10)	0.60(6)		2.8(10)	0.47(6)	
3	46.26					2.4(10)	−0.45(10)	
4	46.64	$(^3P)4s\ ^4P_{1/2,3/2}$	54(5)	0.08(8)		56(5)	0.05(7)	
5	47.19	$(^3P)4s\ ^2P_{1/2,3/2}$	47(8)	0.17(8)		71(8)	0.12(5)	
6	48.33		2.2(3)	0.38(7)		1.8(3)	0.33(7)	
7	48.51		1.4(5)	0.72(6)		1.2(3)	0.42(7)	
8	49.65		3.6(5)	0.47(6)		3.7(4)	−0.12(9)	
9	50.36	$(^1P)4s\ ^2P_{1/2,3/2}$	100	0.28(7)	−0.03(9)	100	0.08(8)	0.09(5)
10	51.35		13(2)	−0.34(10)		1.8(4)	−0.79(12)	

TABLE II. Calculated intensities and angular anisotropy parameters for the resonant Auger transitions following the $2p_{3/2} \rightarrow 4s$ excitation.

	MC				IC				NRL			
Final state	Intensity		β		Intensity		β		Intensity		β	
	0.24		0.03									
	1.44		0.02									
$(^3P)4s\ ^4P_{5/2}$					0.0		−1.00		0.0		−1.00	
$(^3P)4s\ ^4P_{3/2}$	69.7	85	0.02	0.02	32.7	39	0.02	0.02	0.5	1	0.01	0.01
$(^3P)4s\ ^4P_{1/2}$	14.9		0.03		6.2		0.03		0.1		0.01	
$(^3P)4s\ ^2P_{3/2}$	151.2		−0.06		53.1		−0.07		73.6		−0.02	
		186		−0.07		63		−0.08		107		−0.02
$(^3P)4s\ ^2P_{1/2}$	34.9		−0.11		10.3		−0.14		33.1		−0.03	
	5.0		−0.05									
	2.5		−0.32									
$(^1P)4s\ ^2P_{3/2}$	8.2		−0.43		14.9		−0.43		58.8		−0.15	
		100		−0.06		100		−0.10		100		−0.14
$(^1P)4s\ ^2P_{1/2}$	91.8		−0.03		85.1		−0.04		41.2		−0.12	
	6.8		−0.03									

mental value than is that obtained in the intermediate coupling. The mixing of the $3s^13p^54s$, $3s^13p^53d$, $3p^34s^13d^1$, and $3p^33d^2$ configurations produces a completely different fine structure in the calculated resonant Auger spectrum. Some weak peaks can be seen on the lower binding energy side of the $3s^13p^5(^3P)4s$ and around the $3s^13p^5(^1P)4s$ peaks. The biggest difference due to the mixing of configurations is the satellite structure in the binding energy region of 57–60 eV. These lines can also be seen in the experimental spectrum. The peaks at binding energies of about 56.1 and 52.4 eV originate from the shake-up transitions to the $3s^13p^5(^3P)5s$ and $3s^13p^5(^1P)5s$ states [12], which are not included in the calculations. The relative intensities and angular anisotropy parameters for the peaks obtained from different calculation methods are given in Tables II and III.

The $3s^13p^5(^3P)4s$ peak is composed of several components, the average of which is given in Table I. The basis set used in the MC calculations cannot reproduce the structure around the $3s^13p^5(^3P)4s$ state correctly, whereas it is sufficient to produce the satellite structure in the binding energy region of 57–60 eV. The calculated intensities of the resonant Auger and the satellite lines deviate in part strongly from the experimental values. This indicates that the basis set used in the calculations was not large enough. It can be concluded that the energy and intensity distribution of the $2p^{-1}4s \rightarrow 3s^13p^54s$ resonant Auger spectra are very sensi-

TABLE III. Calculated intensities and angular anisotropy parameters for the resonant Auger transitions following the $2p_{1/2} \rightarrow 4s$ excitation.

	MC				IC				NRL			
Final state	Intensity		β		Intensity		β		Intensity		β	
	0.3		0.04									
	1.9		0.03									
$(^3P)4s\ ^4P_{5/2}$					0.0		−0.99		0.0		−1.00	
$(^3P)4s\ ^4P_{3/2}$	84.5	104	0.03	0.03	42.5	51	0.04	0.04	71.8	86	0.01	0.01
$(^3P)4s\ ^4P_{1/2}$	19.2		0.04		8.1		0.05		14.4		0.01	
$(^3P)4s\ ^2P_{3/2}$	24.5		−0.09		14.8		−0.08		1.3		0.02	
		80		−0.06		47		−0.05		10		0.00
$(^3P)4s\ ^2P_{1/2}$	55.3		−0.04		31.7		−0.03		8.9		0.00	
	0.0		1.13									
	7.1		−0.04									
$(^1P)4s\ ^2P_{3/2}$	86.4		−0.04		88.7		−0.05		40.8		0.04	
		100		0.00		100		0.00		100		0.07
$(^1P)4s\ ^2P_{1/2}$	13.6		0.26		11.3		0.36		59.2		0.09	
	1.3		0.24									

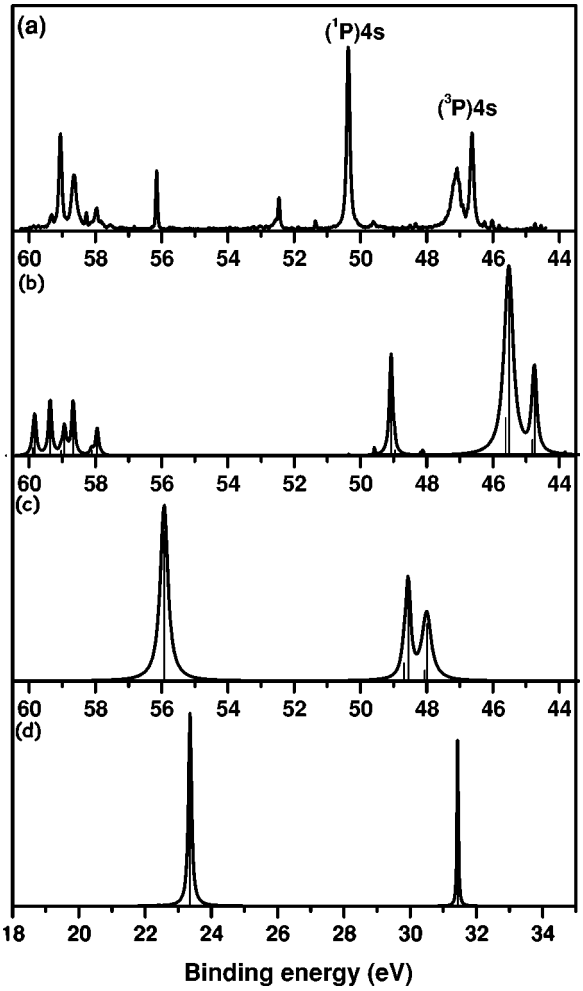

FIG. 2. The experimental $2p_{3/2}^{-1}4s \rightarrow 3s^1 3p^5 4s$ resonant Auger spectrum (a) in comparison with calculations with (b) MC, (c) intermediate coupling, and (d) calculation in nonrelativistic limit.

tive to the calculation method.

The effects of the mixing of configurations on the β parameters of the $3s^1 3p^5(^3P)4s$ and $3s^1 3p^5(^1P)4s$ lines are nevertheless quite small. At the $2p_{3/2} \rightarrow 4s$ resonance, the calculated angular anisotropy parameter for the $(^1P)4s$ line is -0.06. This parameter approaches the experimental result when the IC and, furthermore, the MC method is used. It remains negative, however, whereas the experimental angular anisotropy parameter is positive. Our experimental value is in agreement with the previous study [26].

At the $2p_{1/2} \rightarrow 4s$ resonance the calculated β parameter for the $(^1P)4s$ peak is zero. The previously determined experimental value for the β parameter of the $(^1P)4s$ peak is negative [26] and thus there is a contradiction between the previous and present values. In the resonant Auger spectrum, there is a peak at the binding energy of 51.35 eV. The angular anisotropy parameter of this line is negative. If the kinetic energy resolution is not high enough to resolve this structure in the resonant Auger spectrum, its angular distribution decreases the apparent β value of the transition to the $(^1P)4s$ state. Our MC calculation identifies the peak to be 62.9% of $3p^3 3d^2$, 32.9% of $3p^3 4s 3d$, 2.7% of $3s^1 3p^5 4s$, and 1.5% of $3s^1 3p^5 3d$ character. In their study of inner valence-shell satellites, Combet-Farnoux *et al.* [27] calculated that the peak is 66% of $3s^2 3p^3 3d^2$ and 27.4% of $3s^1 3p^5(^1P)3d$ character. Despite the different identification, it can be assumed that the $3d$ contribution to the peak is very strong. The energy difference between the $2p_{1/2}^{-1}4s$ and $2p_{3/2}^{-1}3d$ resonances in the absorption spectrum of Ar is only 0.42 eV and the resonances are partly overlapping [19,28]. Thus the excitation to the $2p_{3/2}^{-1}3d$ resonant state already takes place to some extent at the maximum of the $2p_{1/2}^{-1}4s$ resonance, no matter how high the photon energy resolution is. When a wider photon band is used in the experiment, the $2p_{3/2}^{-1}3d$ state is excited with higher probability and the intensity of the peak at binding energy 51.35 eV grows. We studied the effect of the different relative populations of the $2p_{3/2}^{-1}3d$ and $2p_{1/2}^{-1}4s$ states by measuring the $2p_{1/2}^{-1}4s \rightarrow 3s^1 3p^5 4s$ resonant Auger spectra at photon energies 246.5 eV, 246.6 eV, and 246.7 eV. The spectra are shown in Fig. 3. When the photon energy grows, the intensity of the peak at binding energy 51.35 eV increases remarkably. It can therefore be expected that the width of the photon band used in the measurement affects the determination of the β value of the $(^1P)4s$ state, if the kinetic energy resolution in the resonant Auger spectrum is not good enough.

TABLE IV. Calculated and experimental intensities for the cascade process.

			Interference			Two-step		
Excitation	Final state	Expt.	MC	IC	NRL	MC	IC	NRL
$2p_{3/2} \rightarrow 4s$	$3p^4\ ^3P_2$	1.0	1.0	1.0	1.0	1.0	1.0	1.0
	$^3P_1$	1.5(2)	1.5	1.4	2.6	1.7	1.2	0.7
	$^3P_0$	0.5(1)	0.6	0.6	3.2	0.7	0.5	0.4
	$^1D_2$	0.7(2)	0.2	5.7	16.0	0.5	5.3	0.9
	$^1S_0$		0.0	1.4	4.0	0.3	1.3	0.3
$2p_{1/2} \rightarrow 4s$	$3p^4\ ^3P_2$	1.0	1.0	1.0	1.0	1.0	1.0	1.0
	$^3P_1$	0.5(1)	0.5	0.5	2.5	0.5	0.4	0.9
	$^3P_0$	0.1(1)	0.2	0.1	2.3	0.2	0.1	0.3
	$^1D_2$	0.4(1)	0.2	3.7	13.4	0.5	3.6	0.3
	$^1S_0$		0.0	0.9	3.4	1.5	0.9	0.1

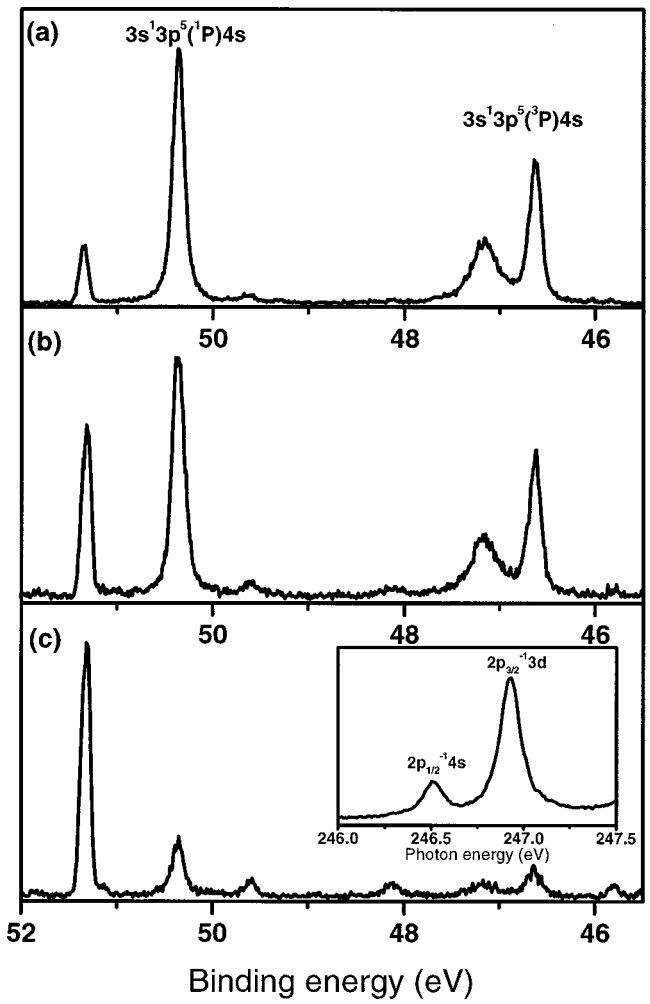

FIG. 3. The experimental $2p_{1/2}^{-1}4s \rightarrow 3s^1 3p^5 4s$ resonant Auger spectra excited at (a) $h\nu = 246.5$ eV, (b) $h\nu = 246.6$ eV, and (c) $h\nu = 246.7$ eV. The absorption spectrum of Ar [19] is shown in the inset of panel (c).

B. The second-step Auger decay

1. Experimental results

The second-step Auger spectra measured at the angles 0° and 90° are shown in Fig. 4. The displayed kinetic energy region of 4.5–7.5 eV corresponds to the Auger decay of the $3s^1 3p^5(^1P)4s$ state to the $3p^4(^1D, ^3P)$ states. The transition to the $3p^4(^1S_0)$ state was not observed. In order to determine the angular anisotropy parameters of the transitions, the spectra were least squares fitted using Voigt functions. The experimental intensities and β parameters for the cascade process are given in Tables IV and VI below.

2. Results of calculations and comparison with experiment

The NRL calculation predicts that the transition rates to the $3s^1 3p^5(^1P)4s(^2P_{1/2})$ and $(^2P_{3/2})$ states are nearly the same, but in the IC approach the rate to the $3s^1 3p^5(^1P)4s(^2P_{1/2})$ state is clearly dominating. In the MC model the transition rate to the $(^1P)4s(^2P_{3/2})$ state is only a few percent of the transition rate to the $(^1P)4s(^2P_{1/2})$ state.

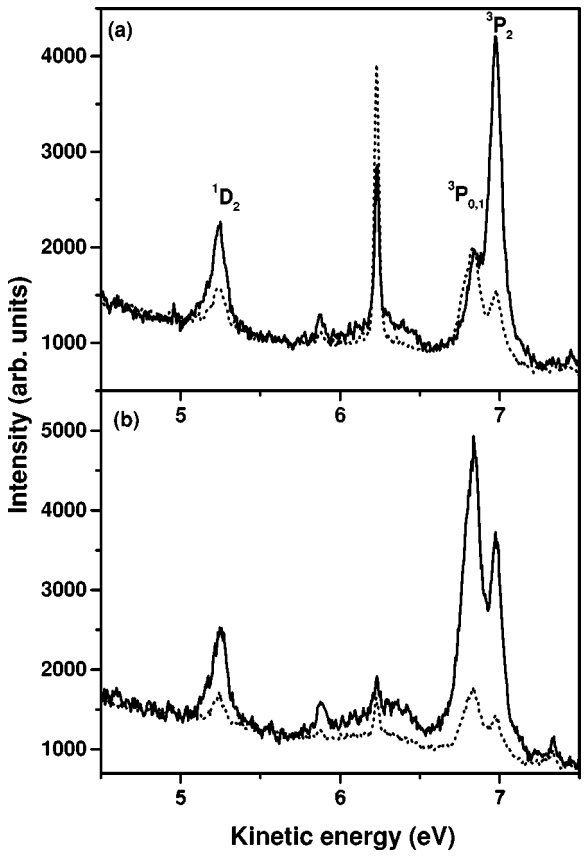

FIG. 4. The experimental second-step Auger spectra of Ar measured at photon energies (a) 246.5 eV corresponding to the Ar $2p_{1/2} \rightarrow 4s$ excitation and (b) 244.4 eV corresponding to the Ar $2p_{3/2} \rightarrow 4s$ excitation. The spectra were measured at 90° (solid line) and 0° (dotted line) upward from the electric vector of the incident light.

The $2p_{3/2}^{-1}4s$ excited state thus decays mainly via the $3s^1 3p^5(^1P)4s(^2P_{1/2})$ state. The excited state $2p_{1/2}^{-1}4s$, however, decays mainly via the $(^1P)4s(^2P_{3/2})$ state (the intensity ratio in the MC calculation is $^2P_{3/2}:{}^2P_{1/2} = 1:0.19$).

The relative intensities calculated for the second-step Auger transitions using the three different approaches are given in Table IV. The mixing of configurations and the interference effect do not change the intensity distribution of the $3p^4(^3P)$ states much from that of the two-step IC approximation, but the NRL limit with interference differs somewhat from the other predictions. The $(^1D_2)$ state is, however, much more sensitive to the calculation method. In the intermediate coupling, the relative intensity of the $(^1D_2)$ state is clearly too high at both resonances and in both type of cal-

TABLE V. Calculated and experimental natural linewidths for the $3s^1 3p^5(^1P)4s(^2P_{1/2,3/2})$ state using the two-step model.

Initial state	Expt. (meV)	Calc. (meV)		
		MC	IC	NRL
$2p_{3/2}^{-1}4s$	92	99	275	41
$2p_{1/2}^{-1}4s$	90	159	281	41

TABLE VI. Calculated and experimental angular anisotropy parameters for the cascade process.

				Interference			Two-step		
Excitation	Final state	Expt.	Expt. [15],[16]	MC	IC	NRL	MC	IC	NRL
$2p_{3/2}\rightarrow 4s$	$3p^4\ ^3P_2$	−0.45(5)		−0.15	−0.22	−0.35	−0.13	−0.20	−0.63
	$^3P_1$	−0.6(2)		−0.12	−0.17	−0.44	0.00	0.00	0.00
	$^3P_0$	−0.3(2)		−0.14	−0.14	−0.73	0.03	0.03	0.26
	$\Sigma(^3P)$	−0.5(1)	−0.44(5)	−0.14	−0.18	−0.56	−0.03	−0.07	−0.27
	$^1D_2$	−0.2(1)		0.09	0.04	0.11	0.00	0.01	0.06
	$^1S_0$			0.83	0.41	1.12	0.94	0.16	0.58
$2p_{1/2}\rightarrow 4s$	$3p^4\ ^3P_2$	−0.50(5)		−0.55	−0.57	0.49	−0.73	−0.75	−0.51
	$^3P_1$	0.7(1)		0.44	0.43	0.37	0.04	−0.03	0.00
	$^3P_0$	1.5(1)		1.16	1.17	−0.17	0.66	0.62	0.15
	$\Sigma(^3P)$	0.0(1)	0.12(7)	−0.06	−0.12	0.18	−0.34	−0.45	−0.21
	$^1D_2$	−0.1(1)		0.21	0.01	−0.03	0.02	0.08	0.04
	$^1S_0$			1.01	0.31	−0.35	1.00	0.90	0.40

culation (the two-step model and the inclusion of the lifetime interference effect). The NRL calculation with interference heavily overestimates the intensity of this state. The intensities obtained from the MC calculation including the lifetime interference effect agree best with the experiment.

The results for the natural linewidth of the $3s^13p^5(^1P)4s(^2P_{1/2,3/2})$ states obtained from different calculations using the two-step model are given in Table V. The experimental linewidths are obtained from the second-step Auger spectra. The linewidths predicted with the MC method are much smaller than with the IC approach. This is caused by the decrease of the absolute transition rate to the $3p^4(^1D_2)$ state. The absolute rate of the $(^1P)4s(^2P_{3/2})\rightarrow 3p^4(^1S_0)$ transition is clearly overestimated in the MC approach. This may cause the big discrepancy between the experimental and calculated linewidths of the $3s^13p^5(^1P)4s(^2P_{1/2,3/2})$ state at the $2p_{1/2}^{-1}4s$ resonance. Excluding the transition rate to the $3p^4(^1S_0)$ state, the linewidths are 93 meV for the $2p_{3/2}\rightarrow 4s$ excitation and 95 meV for the $2p_{1/2}\rightarrow 4s$ excitation, which are in good agreement with experiment. The intensity of the $3p^4(^1S_0)$ line, however, decreases when the interference effect is included (Table IV). This indicates that the two-step description is not capable of predicting the natural widths of the cascade Auger lines.

A state with the total angular momentum $J\leqslant 1/2$ decays isotropically and so the β parameters of all final states in the cascade following the $2p_{3/2}$ excitation, which decay mainly via the $^2P_{1/2}$ state, are close to zero. The calculated β parameters are shown in Table VI. The interference effect changes the angular anisotropy parameters greatly, whereas the effect due to the mixing of configurations is small. For most of the peaks the β parameters obtained with MC and IC approximations, and including the interference effect, are in better agreement with the experimental results than the other predictions. There is, however, a quite large discrepancy between the MC calculations and experimental values for $3p^4(^3P)$ peaks in the second step. Somewhat surprisingly, the agreement is better at the $2p_{1/2}^{-1}4s$ resonance than at the $2p_{3/2}^{-1}4s$ resonance.

The analysis in [16] was done by assuming that only the p wave contributes in the second step, as it is the only contributing wave in the LSJ approximation. Our computations, however, suggest that the f wave is also present in the second step of the cascade. This can be attributed to CI which mixes the first-step final states having $3s^13p^54s$ and $3p^33d^14s$ occupations. These decay to $3p^4$ final states through the Auger amplitudes $\langle 3s\varepsilon l||r_{12}^{-1}||3p4s\rangle$ and $\langle 3p\varepsilon l||r_{12}^{-1}||4s3d\rangle$, respectively. The latter amplitudes give rise to f continuum waves in addition to p waves. According to the MC calculations, the contribution of the f wave can be quite large. In the $(^2P_{1/2})\rightarrow 3p^4(^3P_2)$ transition especially the ratio of the f and p amplitudes is 34% and in the $(^2P_{1/2})\rightarrow 3p^4(^1D_2)$ transition 74%.

3. Breakdown of the LSJ approximation

Previous analyses of the cascade spectra have been made using the LSJ approximation [15,16]. To state briefly, in that case the jj coupled amplitudes are written in the LS scheme using the relation (see, e.g., [29])

$$\langle (L_fS_f)J_f,(l\tfrac{1}{2})j{:}J||V||(L_iS_i)J\rangle = \hat{J}\hat{J}_f\hat{j}\hat{S}_i\begin{Bmatrix} L_f & S_f & J_f \\ l & 1/2 & j \\ L_i & S_i & J \end{Bmatrix}\langle L_fl{:}L_i||V||L_i\rangle. \quad (8)$$

The decay amplitude on the right-hand side of Eq. (8) no longer depends on j. When this is applied to Eq. (6) the summation over the continuum angular momenta involves only the coupling coefficients and can be performed. This simplifies the algebra considerably as the number of amplitudes is reduced. However, the true atomic states can seldomly be described using one LS coupled state only. CI mixes states with the same J value, which may correspond to more than one value of the L and S quantum numbers. In the

TABLE VII. Calculated ratios of the *s* and *d* Auger decay amplitudes and their phase differences for the $2p_{3/2}^{-1}4s \rightarrow 3s^1 3p^5 4s(^2P)$ resonant Auger transitions.

		M_d/M_s			$\cos\Delta\phi$		
Excitation	Final state	MC	IC	NRL	MC	IC	NRL
$2p_{3/2}^{-1} \rightarrow 4s$	$^2P_{3/2}$	0.15	0.15	0.04	−0.94	−0.92	−0.96
	$^2P_{1/2}$	0.01	0.02	0.05	−0.94	−0.93	−0.96
$2p_{1/2}^{-1} \rightarrow 4s$	$^2P_{3/2}$	0.03	0.04	0.05	−0.94	−0.93	−0.96
	$^2P_{1/2}$	0.10	0.14	0.03	−0.94	−0.93	−0.96

presence of CI one thus has to include in both the initial and final states all the *LS* amplitudes corresponding to the chosen *J* value together with the associated mixing coefficients. In this way, the application of Eq. (8) may lead to a large number of recoupled amplitudes and the advantage of its use is lost.

4. The ratio of the s and d Auger decay amplitudes

The calculated ratios of the *s* and *d* Auger decay amplitudes and their phase differences in the resonant Auger transitions $2p_{3/2}^{-1}4s \rightarrow 3s^1 3p^5(^1P)4s(^2P)$ are given in Table VII. The authors of Ref. [16] used an indirect method based on the *LSJ* transformation of the amplitudes to extract the ratio of the *s* and *d* amplitudes and their associated phase difference. Their value for the amplitude ratio was 0.52 ± 0.15 whereas in this work a much smaller value was obtained from the computations. Perhaps more interesting is the phase difference of the amplitudes. According to scattering theory (e.g., [30]), a continuum wave with an orbital angular momentum *l* and a wave number *k* has a phase factor $\exp(i\phi)$ with

$$\phi = l\frac{\pi}{2} + \varphi(k), \tag{9}$$

where $\varphi(k)$ is an energy-dependent factor. For *s* and *d* waves measured at nearly equal energies one thus expects a phase difference $\Delta\phi = \pi + \delta$, where δ is a small number. This gives $\cos\Delta\phi \sim -1$ which is in agreement with the present computations. However, quite a different value was reported in [16] with $\cos\Delta\phi = 0.01 \pm 0.03$. The discrepancies in the amplitude ratio and especially in the relative phase imply a possible defect in the nonrelativistic analysis of [16]. In the present work the amplitude ratio and the phase difference were seen to be almost independent of the effects of CI and electron correlation.

V. CONCLUSIONS

By utilizing the Auger resonant Raman effect it has been possible to resolve the fine structure of the $2p^5 4s \rightarrow 3s^1 3p^5 4s$ resonant Auger spectra in much more detail than before. Present experimental accuracy allowed us to compare the experimental angular anisotropy parameters with theoretical values obtained from different calculations. The Auger cascade process in Ar was found to be very sensitive to the calculation method. Moreover, it was shown that the nonrelativistic scheme is not sufficient for the Ar cascade process. In general, the intensity distributions are more sensitive to the correlation effects than the angular distributions. This may be one reason for the different results between this and the earlier [15,16] work. Only *p* waves were considered in the final states of the second-step Auger decay, especially in Ref. [15]. This seems to be insufficient.

An overall comparison of the MC, IC, and NRL results shows that generally the description of the intensity and angular distributions requires the use of the MC approach. However, even the MC approach still cannot predict all the details of the experimental results. This may be due to an improper account of electron correlation, i.e., too small basis sets in the MC Dirac-Fock calculations. The other source of error may be the omission of the channel interaction, especially in the case of the $^3P_{0,1,2}$ final states of the cascade process.

ACKNOWLEDGMENTS

We are grateful to N. M. Kabachnik for discussions and comments in the earlier part of this work and to the staff of the MAX laboratory for help during the measurements. Financial support from the Vilho, Yrjö, and Kalle Väisälä Foundation (S.-M.H.), from the National Graduate School in Materials Physics (M.J.), and from the Research Council of the Academy of Finland is acknowledged.

[1] M. H. Chen, Phys. Rev. A **47**, 3733 (1993).
[2] J. W. Cooper, Phys. Rev. A **39**, 3714 (1989).
[3] T. A. Carlson, D. R. Mullins, C. E. Beall, B. W. Yates, J. W. Taylor, D. W. Lindle, and F. A. Grimm, Phys. Rev. A **39**, 1170 (1989).
[4] U. Becker, in *Sixteenth Annual Conference on the Physics of Electronic and Atomic Collisions*, edited by A. Dalgarno, R. S. Freund, P. M. Koch, M. S. Lubell, and T. B. Lucatorto, AIP Conf. Proc. No. 205 (AIP, New York, 1990), p. 162.
[5] H. Aksela and J. Mursu, Phys. Rev. A **54**, 2882 (1996).
[6] H. Aksela, J. Mursu, J. Jauhiainen, E. Nõmmiste, J. Karvonen, and S. Aksela, Phys. Rev. A **55**, 3532 (1997).
[7] E. J. McGuire, Phys. Rev. A **11**, 1880 (1975).
[8] J. M. Crotty and F. P. Larkins, J. Phys. B **9**, 881 (1976).

[9] K. G. Dyall and F. P. Larkins, J. Phys. B **15**, 2793 (1982).
[10] O. M. Kvalheim, Chem. Phys. Lett. **98**, 457 (1983).
[11] H. Pulkkinen, Department of Physics, University of Oulu, Report No. 123, 1993 (unpublished).
[12] A. Kikas, S. J. Osborne, A. Ausmees, S. Svensson, O.-P. Sairanen, and S. Aksela, J. Electron Spectrosc. Relat. Phenom. **77**, 241 (1996).
[13] S. Svensson, B. Eriksson, N. Mårtenson, G. Wendin, and U. Gelius, J. Electron Spectrosc. Relat. Phenom. **47**, 327 (1988).
[14] E. von Raven, M. Meyer, M. Pahler, and B. Sonntag, J. Electron Spectrosc. Relat. Phenom. **52**, 677 (1990).
[15] K. Ueda, Y. Shimizu, N. M. Kabachnik, I. P. Sazhina, R. Wehlitz, U. Becker, M. Kitajima, and H. Tanaka, J. Phys. B **32**, L291 (1999).
[16] K. Ueda, Y. Shimizu, H. Chiba, Y. Sato, M. Kitajima, H. Tanaka, and N. M. Kabachnik, Phys. Rev. Lett. **83**, 5463 (1999).
[17] R. Nyholm, S. Svensson, J. Nordgren, and A. Flodström, Nucl. Instrum. Methods Phys. Res. A **246**, 267 (1986); S. Aksela, A. Kivimäki, R. Nyholm, and S. Svensson, Rev. Sci. Instrum. **63**, 1252 (1992).
[18] N. Mårtensson, P. Baltzer, P. A. Brühwiler, J.-O. Forsell, A. Nilsson, A. Stenborg, and B. Wannberg, J. Electron Spectrosc. Relat. Phenom. **70**, 170 (1994).
[19] O.-P. Sairanen, A. Kivimäki, E. Nõmmiste, H. Aksela, and S. Aksela, Phys. Rev. A **54**, 2834 (1996).
[20] G. S. Brown, M. H. Chen, B. Crasemann, and G. E. Ice, Phys. Rev. Lett. **45**, 1937 (1980); G. B. Armen, T. Åberg, J. C. Levin, B. Crasemann, M. H. Chen, G. E. Ice, and G. S. Brown, *ibid.* **54**, 1142 (1985); A. Kivimäki, A. Naves de Brito, S. Aksela, H. Aksela, O.-P. Sairanen, A. Ausmees, S. J. Osborne, L. B. Dantas, and S. Svensson, *ibid.* **71**, 4307 (1993).
[21] C. E. Moore, *Ionization Potentials and Ionization Limits Derived from the Analyses of Optical Spectra* (U.S. GPO, Washington, DC, 1970); *Atomic Energy Levels as Derived by the Analysis of Optical Spectra*, Vol. I (U.S. GPO, Washington, DC, 1971).
[22] K. G. Dyall, I. P. Grant, C. T. Johnson, F. A. Parpia, and E. P. Plummer, Comput. Phys. Commun. **55**, 425 (1989).
[23] J. Tulkki, N. M. Kabachnik, and H. Aksela, Phys. Rev. A **48**, 1277 (1993).
[24] J. Tulkki, T. Åberg, A. Mäntykenttä, and H. Aksela, Phys. Rev. A **46**, 1357 (1992).
[25] N. M. Kabachnik, J. Tulkki, H. Aksela, and S. Ricz, Phys. Rev. A **49**, 4653 (1994).
[26] K. Ueda, Y. Shimizu, H. Chiba, Y. Sato, M. Kitajima, H. Tanaka, S.-M. Huttula, H. Aksela, I. P. Sazhina, and N. M. Kabachnik, in *X-ray and Inner Shell Processes*, edited by R. W. Dunford, D. S. Gemmel, E. P. Kanter, B. Krässig, S. H. Southworth, and L. Young AIP Conf. Proc. No. 506 (AIP, New York, 1999), p. 148.
[27] F. Combet-Farnoux, P. Lablanquie, J. Mazeau, and A. Huetz, J. Phys. B **33**, 1597 (2000).
[28] O.-P. Sairanen, A. Kivimäki, E. Nõmmiste, A. Naves de Brito, H. Aksela, and S. Aksela, MAX-LAB Activity Report 1995, p. 200, 1996 (unpublished).
[29] N. M. Kabachnik, I. P. Sazhina, and K. Ueda, J. Phys. B **32**, 1769 (1999).
[30] T. Åberg and G. Howat, *Corpuscles and Radiation in Matter I*, Vol. 31 of *Handbuch der Physik*, edited by S. Flügge and W. Mehlhorn (Springer, Berlin, 1982), p. 469.